

GT2011-46468

**ACTIVE FLOW CONTROL CONCEPTS ON A  
HIGHLY LOADED SUBSONIC COMPRESSOR CASCADE:  
RÉSUMÉ OF EXPERIMENTAL AND NUMERICAL RESULTS**

**Christoph Gmelin\*,  
Vincent Zander,  
Martin Hecklau,  
Frank Thiele,  
Wolfgang Nitsche**

Technische Universität Berlin  
Strasse des 17. Juni 135  
10623 Berlin, Germany  
Email: christoph.gmelin@cf.d.tu-berlin.de

**André Huppertz,  
Marius Swoboda**

Rolls-Royce Deutschland Ltd. & Co. KG  
Eschenweg 11, Dahlewitz  
15827 Blankenfelde-Mahlow, Germany  
Email: andre.huppertz@rolls-royce.com

**ABSTRACT**

*The paper presents experimental and numerical results for a highly loaded, low speed, linear compressor cascade with active flow control. Three active flow control concepts by means of steady jets, pulsed jets, and zero mass flow jets (synthetic jets) are investigated at two different forcing locations, i.e. at the end walls and the blade suction side. Investigations are performed at the design incidence for jet-to-inlet velocity ratios from approximately 0.7 to 3.0 and two different Reynolds numbers. Detailed flow field data are collected using a five-hole pressure probe, pressure tabs on the blade surfaces, and time-resolved particle image velocimetry. Unsteady Reynolds-Averaged Navier-Stokes simulations are performed for a wide range of flow control parameters. The experimental and numerical results are used to understand the interaction between the jet and the passage flow. Variation of jet amplitude, forcing frequency, and blowing angle of the different control concepts at both locations allows determination of beneficial control parameters and offers a comparison between similar control approaches. The paper combines the advantages of an expensive but accurate experiment and a fast but limited numerical simulation.*

**NOMENCLATURE**

$c_p$	1	pressure coefficient
$F^+$	1	reduced frequency
$h$	m	blade height
$l$	m	chord length
$Ma$	1	Mach number
$p_t$	Pa	total pressure
$p$	Pa	static pressure
$q$	Pa	dynamic pressure
$Re_l$	1	chord based Reynolds number
$S$	m	total length of blade suction side
$t$	m	pitch
$V$	m/s	velocity
$\hat{V}$	m/s	peak velocity
$\bar{V}$	m/s	mean velocity
$x, y, z$	m	coordinate system
$\alpha$	deg	flow angles
$\eta$	1	efficiency
$\Delta p/q_1$	1	static pressure rise
$\gamma$	deg	stagger angle
$\zeta_{q1}$	1	total pressure loss
$\rho$	kg/m <sup>3</sup>	density
$\varphi$	deg	blowing angle

\* Address all correspondence to this author.

## INTRODUCTION

The development trend of modern aero engine compressors is marked by a higher power density, i.e. a higher pressure ratio and less weight, which requires reducing the number of stages and increasing the aerodynamic blade loading. The overall performance of an aero engine is driven by the compressor performance. Therefore, advances that reduce weight, parts, fuel consumption, or lower the maintenance costs of the compressor will also reduce the cost of aircraft ownership. Modern axial compressors are highly optimized engine components (e.g. each individual blade is optimized to its individual flow configuration) that must be designed to match a very broad range of operating conditions (e.g. take-off, cruise, landing) in a very efficient and safe manner. Today, passive flow control using blade sweep and dihedral, casing treatment, end wall contouring etc. are well accepted methods to improve the efficiency and/or the surge margin of a multistage axial compressor.

Nevertheless, it is also assumed that Active Flow Control (AFC) applications in turbomachinery have great potential for overall improvement [1]. Compared to passive devices, active devices can be adapted to the current flow situation which is especially important for off-design conditions like take-off or landing where large flow separations can appear. And they can be switched off, e.g. under design condition where the separation regions usually have the smallest extent.

During the last decades, many aerodynamic investigations outside the compressor world have shown that AFC can significantly improve the aerodynamic performance by reducing flow separation, for instance on aircraft wings (see <http://ntrs.nasa.gov>, keywords: wing, active flow control). In these studies, unsteady jets are one of the most used forcing devices. A general overview about active and passive flow control is given by Gad-el-Hak [2]. However, only few active flow control studies have been conducted for axial compressor configurations and they were mostly constrained to low-speed cases. In a recent study, Nerger [3] investigates steady blowing to control the secondary flow regimes of a highly-loaded compressor cascade, whereas Matejka [4] and Zheng [5] use synthetic jets for the reduction of boundary-layer separation. All of these recent studies show promising results.

Within this study AFC is applied to a highly-loaded low-speed compressor cascade with a low blade aspect-ratio where the secondary flow regime is pre-dominant. Modern compressors, especially the last stages, tend to have low aspect ratios. For these configurations the corner stall regime has a major impact on the total pressure loss, the static pressure rise, and the passage blockage.

In the present study AFC is concentrated on unsteady jet forcing because Greenblatt and Wynanski [6] mention that AFC with pulsating momentum flux can be much more effective and efficient as simple steady blowing. Steady jet forcing is only used for comparison reasons.

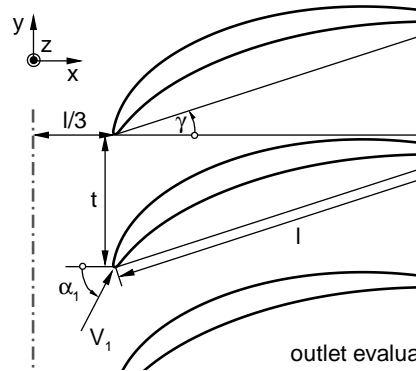


FIGURE 1. CASCADE GEOMETRY.

The major objectives of this study are to investigate the potential of AFC using unsteady jets (with and without mean mass flow) to reduce the secondary flow with very dominant passage vortices and to validate if the trend of the results can be well predicted by URANS computations using commercial CFD codes. The present paper summarizes all findings on active flow control on a highly-loaded compressor cascade within the German National Research Program Sfb 557. It is a résumé of all published results [7–18] which were only possible because of the very close cooperation between the experimental and numerical investigations.

## Apparatus and Procedures

*Rolls-Royce Deutschland* provided the cascade and blade geometry. The blades are designed with an overcritical turning of  $\Delta\alpha = 60^\circ$  and a low aspect ratio of  $AR = 0.8$ . The cascade pitch to chord ratio is  $t/c = 0.4$ . Within the experiment, the cascade consists of seven blades. Since the cascade is designed for axial outflow, the design inflow angle is  $\alpha_1 = 60^\circ$ . In order to obtain a representative Reynolds number despite the low inflow Mach number, the geometry of the cascade is scaled up to a blade height of  $h = 0.3$  m. The according chord length is  $l = 0.375$  m. At the design point, the inflow Mach number is  $Ma_1 = 0.1$ . With respect to the blade chord, the Reynolds number is  $Re_l = 840,000$ . An overview of the cascade geometry is shown in Fig. 1. In addition to the design point, experimental investigations considering synthetic jets are performed at a reduced inflow velocity resulting in an inflow Mach number of  $Ma_1 = 0.07$  and an according Reynolds number of  $Re_l = 600,000$ .

The experiments presented here are conducted at the low speed cascade test facility of the Department of Aeronautics and Astronautics at the Technische Universität Berlin. Figure 2 shows a sketch of the cascade test section. In addition to the seven blades the cascade consists of supplemental tailboards at bottom and top. In front of the tailboards, a boundary layer suc-

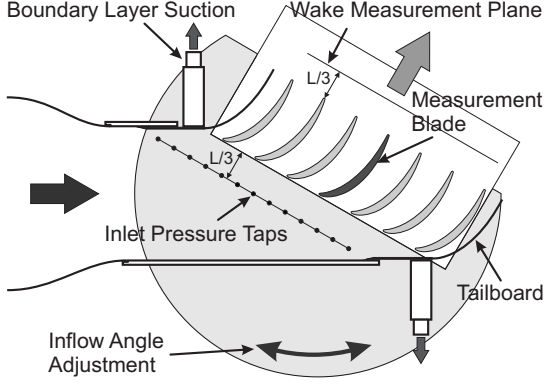


**FIGURE 2.** CASCADE TEST SECTION.

tion is installed to achieve inflow conditions as homogeneously as possible. The suction rate is adjusted corresponding to the static pressure distribution measured in front of the blades.

Three control concepts are considered, namely steady jets, pulsed jets, and zero mass flow (synthetic) jets. Whilst steady jets are characterized by the amplitude of the jet (here the momentum coefficient  $c_{\mu,RMS}$ ) and its direction (the blowing angle  $\varphi$ ), two additional parameters are necessary to define a pulsed jet, i.e. the excitation frequency  $f$  and the duty cycle  $DC$  which specifies the fraction of one cycle the jet is blowing. Synthetic jets represent periodical, sinusoidal forcing with alternating blowing and suction. Thus, they are well-defined by the amplitude of the sine, its frequency, and the direction of the jet during the blowing phase.

Two flow control locations are investigated with regard to the secondary flow pattern of the base flow (cf. Fig. 3). Forcing at the side walls is used to control the dominant secondary flow structures, i.e. the corner vortices, in order to reduce the blockage of the passage. The suction surface flow separation at midspan close to the trailing edge is suppressed by quasi tangential blowing. Both control locations are investigated individually and in combination.

Data evaluation is conducted by means of different parameters and coefficients calculated from the experimental and numerical results. Thus, the passage flow field can be characterized and the actuation depending on the passage flow described. For all data analyses, the evaluation planes are located one third of the chord length upstream of the leading edge and one third downstream of the trailing edge (cf. Fig 1).

The pressure coefficient  $c_p$  is defined as the ratio of the difference of local static pressure  $p_x$  and inlet static pressure  $p_1$  to the dynamic pressure at the inlet  $q_1$ :  $c_p = (p_x - p_1)/q_1$ .

The performance of the stator cascade and the impact of the flow control are determined by the mass-averaged total pressure loss  $\zeta_{q_1}$  (cf. Eq. 1) and the area-averaged static pressure rise  $\Delta p/q_1$  (cf. Eq. 2) analyzed on the evaluation planes over the whole passage. On the basis of the approach proposed by Hartsel [19], who considered cooling jets in a turbine, the pres-

ence of the actuation is respected using a correction term  $\xi$  for each actuator (cf. Eq. 3). The overall correction term  $\xi_{tot}$ , i.e. the sum of the individual ones, is used to calculate the corrected total pressure loss  $\zeta_{q_1,corr}$  (cf. Eq. 4). For synthetic jets, the total pressure loss coefficient needs no correction since they do not add any mass. The momentum flux of the actuator is quantified by  $c_{\mu,RMS}$  (cf. Eq. 5) which represents the momentum of the jet in relation to the momentum of the incoming flow. In order to offer comparison between the different control concepts, the effective value of the jet velocity is considered, which is mathematically represented by the RMS-value  $V_{jet,RMS}$ . For synthetic jets, only the blowing phase of the cycle is respected. In the experiments, the jet velocity is recorded in autonomous investigations and correlated with the situation of the cascade investigation. The remaining parameters are the injected mass flow  $\dot{m}_{jet}$ , the dynamic pressure at the cascade inlet  $q_1$ , and the area of the cascade inlet plane perpendicular to the incoming flow  $A_1 = t \cdot h \cdot \sin(60^\circ)$ .

$$\zeta_{q_1} = \frac{p_{t,1} - p_{t,2}}{q_1} \quad (1)$$

$$\frac{\Delta p}{q_1} = \frac{p_2 - p_1}{q_1} \quad (2)$$

$$\xi = -\frac{\dot{m}_{jet}}{\dot{m}_1} \cdot \left(1 - \frac{V_{jet}}{V_1}\right) \quad (3)$$

$$\zeta_{q_1,corr} = (1 + \xi_{tot}) \cdot \zeta_{q_1} \quad (4)$$

$$c_{\mu,RMS} = \frac{\dot{m}_{jet} \cdot V_{jet,RMS}}{q_1 \cdot A_1} \quad (5)$$

For unsteady concepts, the forcing frequency is normalized by the quotient of the blade chord  $l$  and the inflow velocity  $V_1$ . Thus, the reduced frequency is calculated by  $F^+ = f \cdot l/V_1$ .

The main goal using active flow control in a compressor cascade is to increase the global efficiency. One approach of calculating the efficiency for diffusers is given by Bräunling [20] and can be adapted to the cascade passage for the base flow case. The efficiency relates the benefit to the costs. In a compressor stator, the kinetic energy at the passage outlet  $P_2 = V_2^2/2$  and the specific volumetric work across the passage  $w = \int_1^2 v \cdot dp$  can be seen as benefit. The kinetic energy of the incoming flow  $P_1 = V_1^2/2$  represents the costs. For an efficiency calculation, the cost of the actuation has to be taken into account. The above described efficiency of a diffuser is adapted to the actively controlled compressor stator cascade. The kinetic energy of the actuator jet  $P_{jet} = V_{jet}^2/2$  has to be considered as an additional cost, whilst the specific volumetric work of the injected mass  $w_{jet} = \int_{jet}^2 v \cdot dp$  can be seen as benefit. In order to correctly take the individual impact into account, all parameters are mass flow weighted and the efficiency of a forced cascade flow is calculated as follows.

$$\eta_{AFC} = \frac{\text{benefit}}{\text{costs}} = \frac{P_2 \cdot \dot{m}_2 + w \cdot \dot{m}_1 + w_{jet} \cdot \dot{m}_{jet}}{P_1 \cdot \dot{m}_1 + P_{jet} \cdot \dot{m}_{jet}} \quad (6)$$

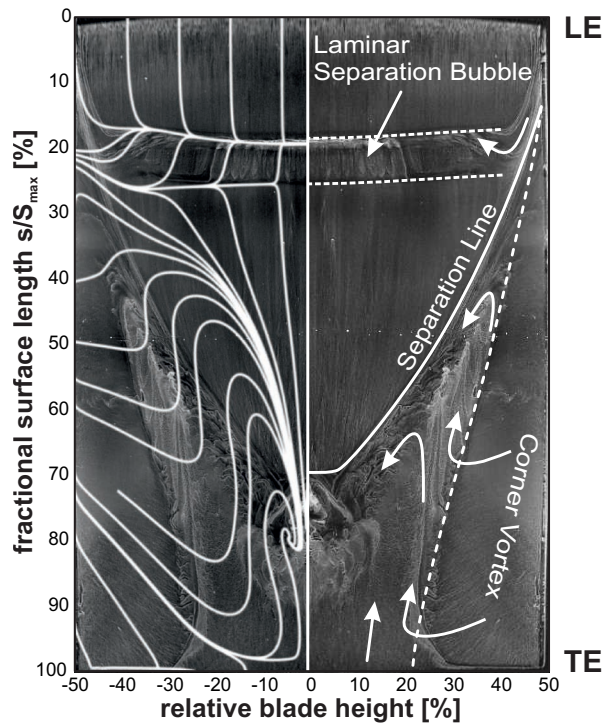


**FIGURE 3.** OIL FLOW VISUALIZATION OF THE BASE FLOW OVERLAID WITH NUMERICALLY CALCULATED WALL SHEAR LINES ON THE LEFT SIDE AND A SKETCH OF THE SECONDARY FLOW PATTERN ON THE RIGHT SIDE.

### Secondary Flow Structures

The secondary flow structures of the suction surface are well presented by an oil flow visualization, depicted in Fig. 3 which is overlaid with numerically calculated wall streamlines defined by wall-shear stresses on the left side and a sketch of the flow pattern on the right side. The air flows from top to bottom and the edges on left and right represent the side walls.

At first, the general flow characteristics will be discussed. The incoming flow separates laminar. Transition from laminar to turbulent occurs over the separation bubble. At the streamwise position of the turbulent reattachment strong secondary flows caused by the end walls come into effect. The main flow is narrowed by the corner vortices in stream-wise direction. Between the secondary and the main flow a 3D separation line is formed ending up at mid-span where the separation is nearly perpendicular to the main flow. In the experiment the laminar separation bubble extends from 17% to 24% suction side length (i.e. from 15% to 21% chord length) and the separation at midspan is observed at approximately 70% suction side length (i.e. 72% chord length). At the trailing edge, the secondary flow extends over 30% of the cascade pitch at midspan (i.e. 0% span). In direction to the wall, the extension in pitch-wise direction increases to 50% of the pitch at approximately 40% span.

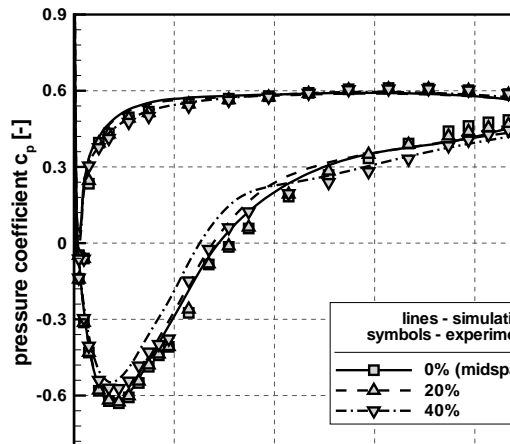


**FIGURE 4.** PRESSURE COEFFICIENT DISTRIBUTION AT 0%, 20%, AND 40% SPAN FOR EXPERIMENT AND SIMULATION.

The described phenomena are well captured by the simulation. Bubble size and position are well predicted by the flow solver. Slight differences can be detected close to the end walls where the numerically computed bubble is of larger size compared to the experiment. A distinct discrepancy is found in the area where the corner vortices emerge from the wall. The predicted secondary flow regime is over-estimated compared to the experiment. A possible reason could be the known limitations of the used linear eddy viscosity model. As a consequence the flow separation at midspan is delayed to 82% suction side length (i.e. 83% chord length) for the computed case.

Further comparison between experiment and simulation is provided in Fig. 4 showing the pressure distribution at 0%, 20%, and 40% blade height. At the blade pressure side, the agreement is good along the span, with a maximum difference of less than 5%. On the suction side, the peak pressure is well predicted by the flow solver along the span. At midspan (0% span), the simulation concurs well with the experimental data until 70% chord length. Downstream, the pressure is underpredicted by approximately 10%. At 20% span, the simulation overpredicts the pressure at around 40% chord length by 15%. Toward the trailing edge, the values are underpredicted by approximately 5%. Close to the wall, at 40% span, the discrepancies increase. The suction peak is less well predicted and the pressure is overestimated by 5 - 10% until midchord. Further downstream the agreement is good, with an underprediction of less than 4% downstream from 70% chord length. Overall, the pressure distribution is well captured by the flow solver. The differences at midspan toward the trailing edge can be related to the delayed separation, and the discrepancies at midchord next to the wall result from the overestimation of the secondary flow within the numerical simulation.

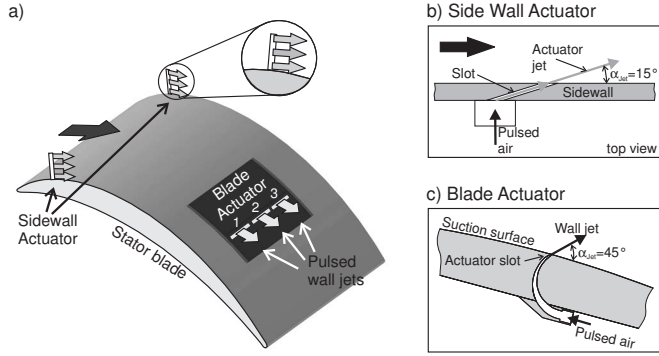


**FIGURE 5.** a) STATOR BLADE WITH ACTUATOR SETUP. b) SIDE WALL ACTUATOR (CROSS-SECTION IN TOP-VIEW). c) BLADE ACTUATOR (CROSS-SECTION).

## STEADY AND PULSED JETS EXPERIMENTS

### Actuator Setup

Based on the complex flow topology in the cascade passages, the flow control approaches are adapted to the dominant flow separations. The cascade is equipped with two different actuator setups (Fig. 5(a)), i.e. the side wall actuator (SW) and the blade actuator (BA). Fast-switching solenoid valves are used for pulsing the compressed air in both actuator concepts, with variation of the frequency, the duty cycle and the amplitude. The side wall actuator is located slightly upstream of the formation of the corner vortices ( $x/l = 10\%$ ). The blowing angle is  $\varphi = 15^\circ$  to the side wall, as it can be seen in Fig. 5(b). The blade actuator is installed within the suction surface at a blowing angle of  $45^\circ$  to the local blade surface and is located just upstream of the separation at midspan ( $x/l = 70\%$ ), cf. Fig. 5(c). The initial jet drives a vortex which transfers fluid from the mean flow to the wall. The jet flaps to the wall and remains attached. A detailed description of the actuator setup is given in [15].

### Steady and Pulsed Jets Results

The secondary flow structures are forced by blowing out of the side walls. The effect of the side wall actuators on the secondary flow structures has already been discussed in [7, 8]. The blockage of the passage flow is reduced by repositioning the corner vortices toward the side wall (cf. Fig. 6). Low frequency forcing with  $F^+ < 0.8$  causes a very unsteady behavior of the entire passage flow. Using higher frequencies, the corner vortex position is more stationary.

The flow separation at the midspan region of the suction surface can be delayed by the blade surface actuator. Due to the pulsed wall jet, high momentum fluid is transferred toward the blade surface which leads to the reattachment of the separated boundary-layer. The separation line is shifted toward the trailing edge and the deflection enlarges. The mechanism of reattachment is well described in [8].

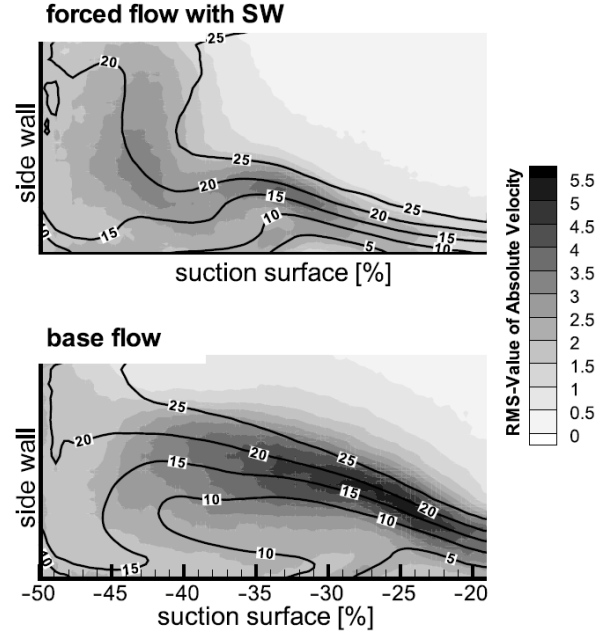


**FIGURE 6.** PIV MEASUREMENTS OF THE CORNER VORTEX AT 70% CHORD OF THE BLADE, WITH ISO-LINES OF THE ABSOLUTE VELOCITY.

Comprehensive parameter studies are undertaken by variation of the actuator parameters and the combination between the actuator concepts, cf. [10]. The injected mass through the actuators with respect to the passage mass flow always is below a mass flow ratio of  $\dot{m}_a/\dot{m}_p = 0.5\%$ . The resulting momentum coefficient for pulsed and steady excitation is set between  $0.6\% < c_{\mu,RMS} \leq 2\%$  and the velocity ratio is between  $2 \leq V_{jet}/V_1 \leq 3.5$ . Fig. 7 and 8 show the reduction of the total pressure loss and the efficiency for each actuator working individually and in combination. Using only the side wall actuators, the largest reduction of the losses can be reached with steady blowing. In contrast to this, pure blade surface blowing only increases the losses. Comparing the efficiency, where the static pressure rise is one of the main impact factors, the best gain can be reached with the blade actuators. So, a contrary trend of reducing the total pressure loss and increasing the static pressure rise is observed.

However, the largest reduction of the total pressure loss can only be achieved if the flow is forced using both actuator concepts in combination. The passage blockage is reduced with the side wall actuators shifting the corner vortices toward the side wall. This leads to a decreased total pressure loss  $\zeta_{q1}$  and an increased static pressure rise  $\Delta p/q_1$  across the stator passage. Additionally, the region of the boundary layer separation at midspan is enlarged in span-wise direction. Thus, the blade actuators suppress the flow separation more efficiently. The diffusion of the

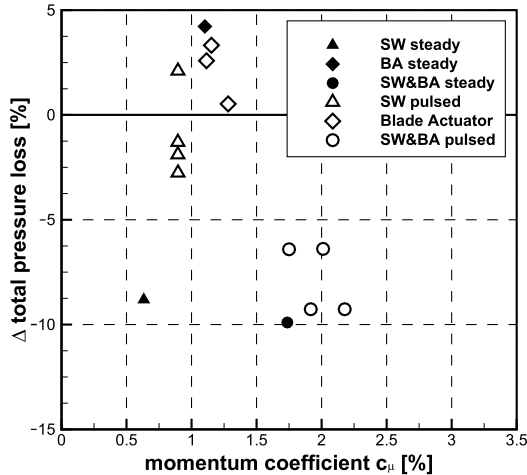


FIGURE 7. TOTAL PRESSURE LOSS FOR STEADY AND PULSED JETS.

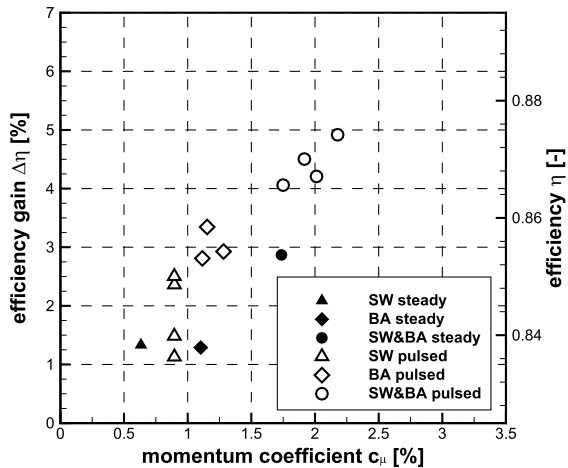


FIGURE 8. EFFICIENCY OF STEADY AND PULSED JETS.

passage increases significantly if both actuator concepts are used in combination. As an example, one of the best actuator parameters for combined forcing at both locations is  $F_{SW}^+ = 1.5$ ,  $F_{BA}^+ = 1.2$  and  $c_{\mu,RMS} = 2\%$ , resulting in a gain in efficiency of up to 5% and a reduction of the total pressure loss by 10%.

## SYNTHETIC JET EXPERIMENTS

The Synthetic Jet (SJ) experiments are conducted at a reduced inflow velocity resulting in a Reynolds number of  $Re_l = 600,000$ . Thus, sufficient jet velocity ratios of up to  $V_{jet}/V_1 = 1$  are reached by the SJ actuators. Compared to the pulsed jets, the injected momentum flux is by an order of magnitude smaller. Nevertheless, comparable loss reductions are achieved using syn-

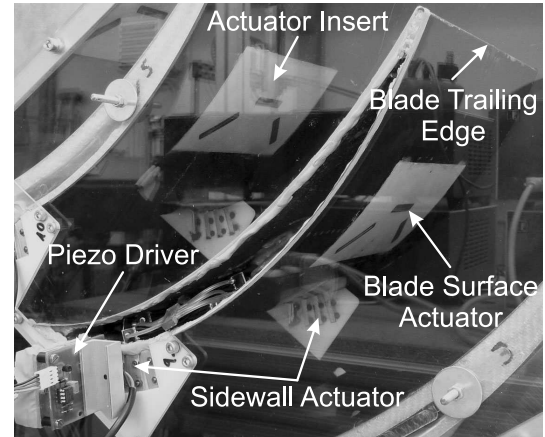


FIGURE 9. SYNTHETIC JET ACTUATOR SETUP

thetic jets. The flow characteristics at the reduced Reynolds number are similar to the above described (cf. Fig. 3). Due to the reduced inflow velocity, the laminar separation bubble now extends from 18% to 26% suction side length (i.e. from 16% to 22% chord length). Reducing the Reynolds number, the corner vortices propagate faster toward midspan and the separation at midspan is shifted upstream to 63% suction side length (i.e. 63% chord length). Since the flow topology for the reduced Reynolds number is equivalent to the design case, the results for the synthetic jet are comparable to the pulsed jet experiments regarding the normalized parameters. As for the pulsed jet experiments, two different control locations are selected for the SJ investigations. Figure 9 shows a picture of the actuator setup. In order to determine the crucial factors for an effective loss reduction, a wide parameter study is conducted. Besides the inflow parameters of the cascade, the jet angle, the jet velocity ratio, and the actuation frequency are varied for different actuator setups. To gather the influence of SJ actuation on the cascade flow, detailed wake and blade surface measurements are conducted. Furthermore, areal measurements of the surface pressure and the wall shear stress are conducted and can be found in [17] and [18].

### Side Wall Actuators

For the flow control experiments, piezo driven synthetic jet actuators are developed [17]. The side wall actuators are mounted at the same axial position as used for the steady and pulsed blowing (i.e. 10% chord length). Even the slot geometry is identical with these configurations. Nevertheless, the injection angle is changed to  $\phi_{SJ} = 35^\circ$  because of constructive reasons.

### Blade Surface Actuators

A second type of synthetic jet actuator is designed for the integration into the blades in order to delay the suction side sep-

separation. Three individual actuators are positioned along the separation line developing for the investigated inflow conditions of  $\alpha_1 = 60^\circ$  and  $Re_l = 600,000$ . The rectangular slots are designed according to the side wall actuators. To cover a larger portion of the blade span, the slot width was increased to  $w = 35$  mm. The actuators are positioned between  $x/l = 59\%$  and  $x/l = 66\%$  along the shape of the separation line. The blowing angle and the maximum jet velocity ratio are equivalent to the side wall actuators ones. To maintain symmetric flow conditions, the actuators are applied symmetrically to all six passages (cf. Fig. 9). A detailed description of the actuators is given in [17].

### Synthetic Jet Results

The SJ experiments performed on the highly loaded compressor cascade reveal that this control approach has the potential to reduce the total pressure loss by weakening the secondary flow structures on the blade surface. Figure 10 shows the relative reduction of total pressure loss plotted over  $c_{\mu,RMS}$ . The reduced jet amplitudes result in a momentum coefficient which is by an order of magnitude smaller compared to the pulsed jets, whereas the relative pressure loss reductions are similar to the results presented before. However, the blade loading is reduced by decreasing the Reynolds number. Nevertheless, the parameter study reveals comparable trends found for both control approaches. A crucial parameter is the positioning of the actuators, since the SJ's add streamwise momentum and increase the mixing between outer flow and boundary layer. The SJ's have to be placed upstream of the separation or developing corner vortex to reveal a positive effect on the flow field. Small blowing angles are more effective for synthetic jets as well. Maximum loss reduction can be achieved using the surface and side wall actuators in combination as can be seen from the results in Fig. 7 and Fig. 10. Most advantageous for the SJ's is a combination of the side wall actuators with both outer blade surface actuators. The center actuator on the blade surface is already positioned downstream of the flow separation and therefore causes an increase of the total pressure loss. In contrast to the pulsed jets, usage of the surface actuators without the side wall actuation causes only slight improvements in the loss reduction. Considering the efficiency presented in Fig. 11, these configurations reveal significant negative efficiency values. A different definition for the efficiency calculation is used for the SJ's, because of the zero net mass flux of the actuator. The Synthetic Jet Actuator (SJA) efficiency is calculated using the energy consumption of the actuator  $W_{SJA}$  and the energy gain  $\Delta W$  resulting out of the loss reduction. The calculation of  $\Delta W$  is based on the changes of the total pressure loss during SJ actuation. A detailed description of  $\eta_{SJA}$  is given in [4] and [17].

$$\eta_{SJA} = \frac{\Delta W - W_{SJA}}{W_{SJA}} \quad (7)$$

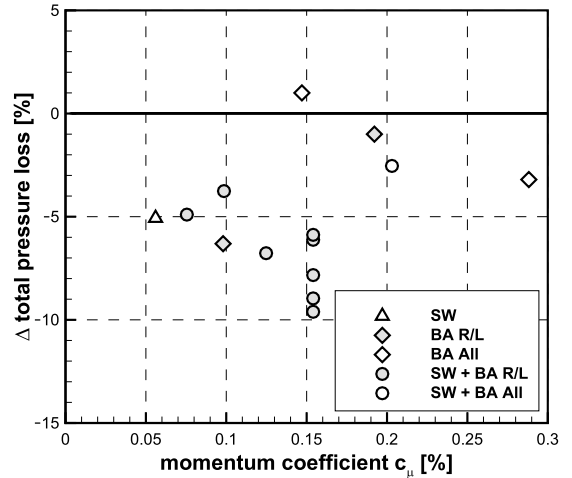


FIGURE 10. TOTAL PRESSURE LOSS FOR SYNTHETIC JETS

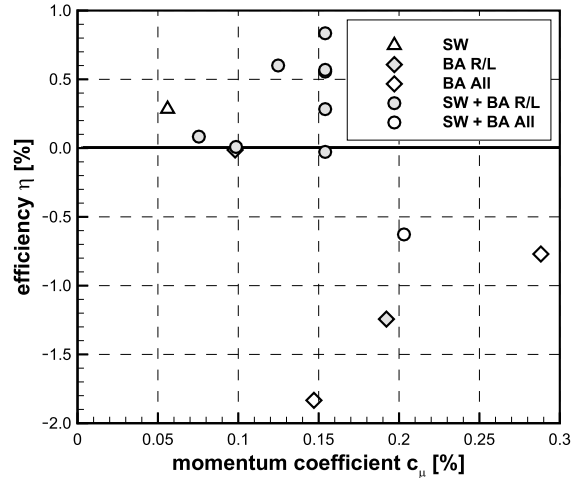


FIGURE 11. EFFICIENCY OF SYNTHETIC JETS

Values of  $\eta_{SJA} > 0$  denote a positive energy balance and negative values an energy loss. Figure 11 shows a significant gain in efficiency for some configurations. The best configuration reaches  $\eta_{SJA} \approx 0.9$  which means that the saved up energy exceeds the energy spent for driving the SJ's by a factor of two.

Additionally, it is observed during the parameter study that the velocity ratio has to exceed a threshold value of  $V_{jet}/V_1 > 0.8$  in order to obtain a positive effect on the flow field [17]. In comparison to local velocities, ratios of  $V_{jet}/V_{SW} \approx 0.8$  are used for the side wall actuators and  $V_{jet}/V_{BA} \approx 1.25$  for the blade actuators, respectively. Besides these global findings some distinct differences to the pulsed jet experiments are also observed. One major advantage of the piezo driven synthetic jets is the ability to

reach higher excitation frequencies. A frequency variation from  $F^+ = 0.6$  up to  $F^+ = 3.8$  reveals a clear frequency dependency of the synthetic jet actuation on the loss reductions [17] which can not be found for the pulsed jet experiments. The appearance of distinct peaks denotes that instabilities inside the flow field can be forced by the synthetic jets which leads to an efficient reduction of the total pressure loss.

### Summary of the Synthetic Jet Experiments

For the SJ's promising loss reductions can be achieved with relatively small momentum coefficients. Furthermore, no net mass flux is needed for the actuation which results in extremely high efficiencies for the synthetic jets. These findings can be confirmed by other investigations on compressor flows presented in [4] and [5]. The small jet velocity ratios below one represent realistic values for an application of the SJ's in a real compressor environment. Besides these advantages there are parameters that make a SJ application into turbomachines difficult. The maximum jet velocities are too small for high Mach number applications. Also the high frequencies of the actuator reduce the life time cycle of the flow control device.

### NUMERICS

All numerical investigations of the compressor cascade are performed at the design point of the profile ( $Ma_1 = 0.1$ ,  $\alpha_1 = 60^\circ$ ,  $Re_l = 840,000$ ). Steady jets, pulsed jets, and synthetic jets are considered by means of (Unsteady) Reynolds-Averaged Navier-Stokes ((U)RANS) simulations at both control locations individually and in combination. For the wide parameter variation more than 150 unsteady RANS simulations are performed.

### Flow Solver

The basic idea of the simulations performed is to validate if the experimental findings can be predicted following an industrial approach realizable within an everyday design process of turbomachinery blades. Thus, the commercially available finite-volume Navier-Stokes solver *FINE<sup>TM</sup>/Turbo v.8.6 - 1* [21] from *NUMECA International*, specialized for turbomachinery application, is employed. The one-equation turbulence model of Spalart-Allmaras (SA model) [22] is used in combination with fixed transition on the blade surfaces. Grids are created with *G3DMESH* [23], a tool developed at DLR Cologne. A more detailed description of the flow solver and the transition modeling can be found in previous publications [12, 14]. The spatial resolution of the passage flow is investigated in [14] by means of a span-wise coarsening and refinement of the mesh by 25% of the grid points. The analysis shows saturated results on the chosen grid. The cascade is meshed with approximately 2.5 million grid cells. The inlet is located 0.8 times the chord length

upstream of the leading edge and the computational domain extends to 2.4 times the chord length downstream of the trailing edge. According to the flow solver and the applied turbulence model, the mesh is block structured and approximately 20 grid lines resolve the boundary layer down to the viscous sublayer. The span-wise direction is resolved with 97 points and the maximum dimensionless wall distance is  $y_{\max}^+ \approx 2$ . Calculation of steady jet cases in RANS mode converge within several hours if computation is run on 8 CPUs with 2.4GHz. A simulation of one parameter set of an unsteady AFC concept on 12 CPUs takes approximately 5 days.

For comparative reasons, the base flow and some selected forced flow cases are simulated using another commercial Navier-Stokes solver, *CFX* from *ANSYS*. Calculations are run on the same meshes with comparable boundary conditions and equivalent temporal discretization. Here, the two-equation  $k-\omega$ -SST turbulence model is used in combination with the  $\gamma-\theta$  transition model. Even though the results of these simulations are not shown in the present paper, it is worth mentioning that they agree very well with the presented calculations and thus fortify the possibility to determine AFC parameter and impact trends using a commercial CFD software within an industrial approach.

### Implementation of AFC

For all control concepts investigated, the actuators are spatially resolved by nozzle block cavities attached to the main computational domain at the respective control locations. Resolution of the slot is realized by locally refining the cascade mesh in the vicinity of the actuation. Even though RANS simulations fail in the prediction of the complex flow phenomena involved in AFC, the results show that the chosen approach represents a practicable solution and provides good agreement with the experimental data. The influence of the temporal discretization of a synthetic jet is investigated within the limits of an industrial approach in [14]. It is shown that even doubling of the time steps or the internal iterations per actuation cycle does not improve the results in an order that would justify the according rise of the computational costs.

### Numerical Results

The base flow case is thoroughly evaluated against experimental data in [12] and [16]. Detailed analysis of the pressure coefficient at several span-wise positions shows that, apart from a greater discrepancy in the shape of the intersection between secondary flow and main flow (cf. Fig. 3 between 20% and 70% suction side length), the complex flow pattern is very well predicted by the flow solver. This concurrence is enforced comparing the three-dimensional flow field of the simulation against PIV data from the experiment [13, 16]. Especially the global performance parameters of the simulation match the experimental values within a difference below 2%.

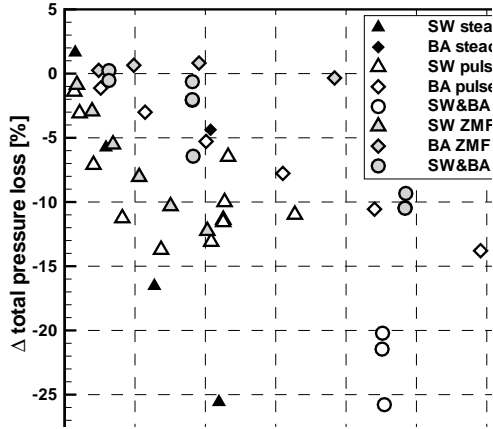


**FIGURE 12.** TOTAL PRESSURE LOSS FOR THE NUMERICAL PARAMETER VARIATION.

The pulsed blowing concept is investigated in [11] for the end wall location and in [13] for the suction side location. A wide variation of forcing parameters is performed for each location individually. Detailed analysis of the local flow fields of the secondary flow phenomena and the interaction mechanism between separated flow and forcing jet are analyzed in [16] by means of experimental PIV data and numerical results for pulsed blowing at both locations individually and in combination. Numerical parameter variations for the synthetic jets can be found in [12, 14].

The representative calculations of the wide parameter variations are selected in order to compare the three control concepts and the two forcing locations against one another and evaluate the predicted trends against the experimental findings. Therefore, the global performance parameters of the cascade are considered by means of the achieved reduction in total pressure loss and the increase in pressure rise with respect to the unforced base flow. The outcome is depicted in Fig. 12 and Fig. 13, respectively.

The major findings of the experimental parameter variation can be observed in the simulation as well. Firstly, unsteady blowing at the side wall with low frequencies ( $F^+ < 0.8$ ) synchronizes the corner vortex movement with the forcing frequency. If the reduced frequency is  $F^+ > 0.8$ , the secondary flow is no longer able to follow the forcing signal and the position of the forced corner vortices is nearly stationary. For higher frequencies, the impact is found to be nearly independent of the excitation frequency. Secondly, the forcing at the blade location is sensitive toward the frequency. If the forcing frequency is small ( $F^+ < 0.5$ ), the flow completely re-separates between two blowing phases. For higher frequencies, the flow remains attached to the suction surface and the losses are significantly reduced. Further details on these phenomena can be found in [7, 13, 16].

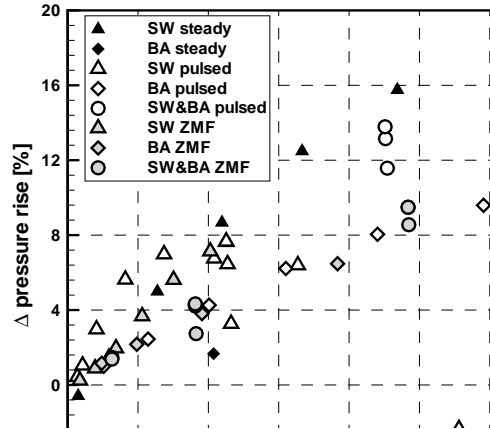


**FIGURE 13.** PRESSURE RISE FOR THE NUMERICAL PARAMETER VARIATION.

Thirdly, a clear trend can be seen for all three concepts that the total pressure loss is reduced and the pressure rise increased with increasing momentum flux. For very small amplitudes ( $0\% \leq c_{\mu,RMS} \leq 0.25\%$ ), the unsteady forcing is more effective than the steady blowing. Pulsed blowing is still more favorable up to a momentum flux of  $c_{\mu,RMS} = 0.5\%$ . The reason is the higher jet velocity of the unsteady forcing during the blowing phase (compared to a steady jet) which mainly drives the impact of the flow control. Fourthly, the actuation at the blade suction surface has less impact on the cascade performance than the side wall forcing if similar momentum fluxes are considered. Fifthly, higher performance values can be reached if the forcing is applied at both locations simultaneously. Of course the effort adds up as well and thus the momentum flux increases compared to individual forcing at one location only. Sixthly, synthetic jets are less effective concerning separation control than pulsed or steady jets. But they do have the advantage that no mean mass flow is needed. Finally, regarding the efficiency of the cascade in Fig. 14, the same trends as observed in the experiments are found. Even though the performance of the cascade is slightly over-estimated by the simulation, the impact of the different control approaches is well captured. Overall, the impact of the various forcing parameters on the trends of total pressure loss, pressure rise, and thus efficiency can be predicted by the simulation in very good agreement to the experiment. The cascade performance parameters are over-estimated by the simulation in most cases, but the efficiency gain is comparable to the experimental one. The same control parameters turn out to be most favorable, e.g. pulsed blowing at both locations in combination with  $F^+ \approx 1.2$  and  $c_{\mu,RMS} \approx 2\%$ . In the simulation, this configuration reduces the losses by 20%, increases the pressure rise by 12%, and results in an efficiency gain of 6%.

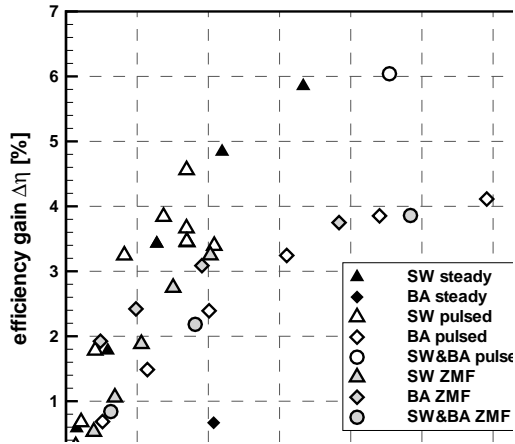


**FIGURE 14.** NUMERICAL EFFICIENCY OF DIFFERENT CONTROL CONCEPTS AND LOCATIONS.

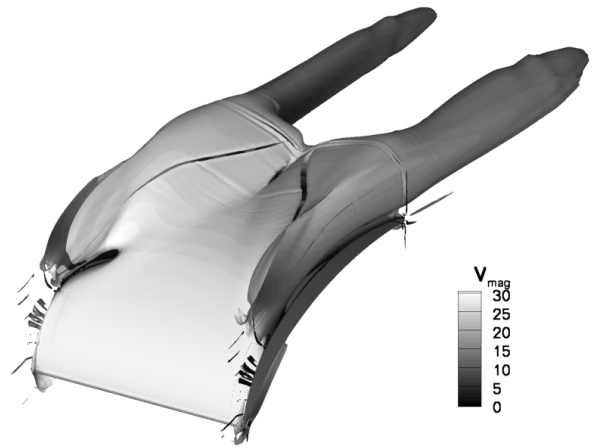
### Flow Visualization

The vortex structures evolving in the passage are visualized by isosurfaces of the  $q$ -criteria introduced by Hunt et al. [24]. Thus, a visual impression of the impact of active flow control on the secondary flow structure is provided in Fig. 15. For the steady base flow simulation (Fig. 15(a)) the dominance of the corner vortices blocking the passage flow and their growing-together resulting in the separation at midspan is nicely illustrated. For the forced flow case, a time-average of pulsed jets at the side wall and the blade surface in combination is shown (Fig. 15(b)). It can be clearly seen that the flow control reduces the magnitude of the corner vortices and forces them toward the side walls. Also visible is the achieved reattachment of the flow separation. The blockage of the passage flow is clearly reduced and the secondary flow structures are less dominant.

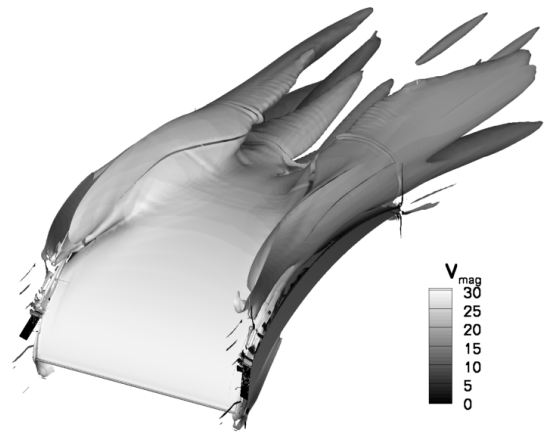
### CONCLUSION

Experimental and numerical investigations are performed on a highly-loaded, low-speed compressor cascade with a low aspect ratio using Active Flow Control (AFC). Three active flow control concepts by means of steady jets, pulsed jets, and synthetic jets are investigated at two different forcing locations to reduce the total pressure loss and to increase the static pressure rise by reducing the corner stall.

Basically, the URANS computations predict the same AFC trend as found by the experiments without resolving the unsteady jets temporally or spatially in detail. However, the Spalart-Allmaras and SST turbulence model overestimate the secondary flow regime which was also found by Lewin et al. [25]. One reason for this can be that linear eddy viscosity models only



(a) STEADY BASE FLOW SIMULATION.



(b) TIME-AVERAGED FORCED FLOW SIMULATION.

**FIGURE 15.** SECONDARY FLOW VISUALIZATION BY ISOSURFACES OF THE  $Q$ -CRITERIA COLOR CODED WITH THE VELOCITY MAGNITUDE.

capture the first order effects of the Reynolds stress anisotropy and streamline curvatures which are strongly pronounced in secondary flow fields.

The experimental and numerical results show that optimal AFC configurations are able to reduce the total pressure loss by 13% and increase the static pressure rise by 9% if a suitable mass flow rate below 0.5% is used. Calculating the efficiency of the compressor cascade respecting the presence of the jet, an increase of up to 5% is reachable.

All pulsed and steady jets need only a small mass flow rate (below 0.5%) to be effective compared to other investigations (e.g. [3, 26]) using mass flow rates above 2%. A mass bleed in an order of some percent is not acceptable for an axial compressor because this will significantly decrease its overall efficiency. Thus, a proper jet nozzle design with a small slot like in this

study is mandatory to reduce the effective mass flow rate of the actuator.

For all AFC configurations, the best forcing location is slightly upstream of the boundary-layer separation which supports the findings of other, more generic AFC investigations (e.g. Gad-el-Hak [2]). Quasi-tangential blowing is the most effective jet direction for all steady and unsteady jets. This also corresponds to the findings of Nerger [3].

The entire flow field has a very steady character, i.e. no dominant frequency was found in the passage that can be used as a forcing frequency. Most effective forcing frequencies for the pulsed and synthetic jets are above  $F^+ > 0.8$ . Pulsed jets have no pronounced frequency, in contrast to synthetic jets which are more frequency sensitive. For low amplitudes, pulsed blowing is more favorable than steady blowing at the same integral momentum flux until saturation is reached. Synthetic jets are slightly less effective than steady or pulsed jets but they do not need any mean mass flow.

It should be noted that the AFC effects are mainly amplitude driven. All jet actuators need at least an amplitude ratio  $V_{jet}/V_1 \geq 1$  to have an impact on the flow field. Thus, jet forcing of the corner separation region is not applicable to first compressor stages where the flow field is transonic. Assuming an inlet Mach number of  $Ma_1 = 0.7$ , amplitude ratios up to 1.4 are realistic which give an efficiency improvement around 2%.

The best actuator configuration is the combined forcing at side wall and suction side. It should be mentioned that suction side blowing is not applicable to the rather thin compressor blades, but it can perhaps be used for engine struts. However, the pure side wall blowing is not much worse than the combined forcing and this is for instance applicable for stator blades at the casing.

In order to validate these forcing parameters (e.g. frequency, amplitude) at high Mach numbers, a high-speed cascade experiment was set up. The investigation has just started.

Major challenges for a real engine application are the robustness and the needed high power density of the jet actuators. However, due to the limited fuel resources and the increasing fuel consumption world-wide, it is only a question of time for the more complex flow control devices to be applied to aero-engine components. The actuator technology will play a key role in this concept.

## ACKNOWLEDGMENT

The results presented were obtained in cooperation with Rolls-Royce Deutschland Ltd. & Co. KG as part of the Collaborative Research Center 557 "Control of turbulent shear flows" at TU Berlin. The authors would like to thank the German Research Foundation (DFG) and Rolls-Royce Deutschland Ltd. & Co. KG for funding this work and permitting the presentation of results.

## REFERENCES

- [1] Lord, W.K., MacMartin, D.G., and Tillman, G., 2000. "Flow Control Opportunities in Gas Turbine Engines". *AIAA Paper 2000-2234*.
- [2] Gad-el-Hak, M., Pollard, A., Bonnet, J.-P., and (Eds.), 1998. "Flow Control: Fundamentals and Practices". *Lecture Notes in Physics*, Springer.
- [3] Nerger, D., 2009. "Aktive Strömungsbeeinflussung in ebenen Statorgittern hoher aerodynamischer Belastung durch Ausblasen". PhD Thesis, Technische Universität Braunschweig.
- [4] Matejka, M., Safarik, P., Popelka, L., and Nozicka, J., 2008. "Influence of active methods of flow control on compressor blade cascade flow". *ASME GT2008-51109*.
- [5] Zheng, X., Zhou, S., Lu, Y., Hou, A., and Li, Q., 2008. "Flow control of annular compressor cascade by synthetic jets". *Journal of Turbomachinery*, **130**(021018), pp. 1–7.
- [6] Greenblatt, D., and Wygnanski, I.J., 2000. "The Control of Flow Separation by Periodic Excitation". *Progress in Aerospace Sciences*, **36**, pp. 487–545.
- [7] Hecklau, M., Zander, V., Nitsche, W., Huppertz, A., and Swoboda, M., 2010. "Active Secondary Flow Control on a Highly Loaded Compressor Cascade by Periodically Pulsating Jets". Dillmann, A., Heller, G., Klaas, M., Kreplin, H.P., Nitsche, W., and Schröder, W., eds., Vol. 108 of *Notes on Numerical Fluid Mechanics and Multidisciplinary Design*, Springer.
- [8] Hecklau, M., van Rennings, R., Zander, V., Nitsche, W., Huppertz, A., and Swoboda, M., 2010. "Particle image velocimetry of active flow control on a compressor cascade". *Experiments in Fluids*.
- [9] Zander, V., Hecklau, M., Nitsche, W., Huppertz, A., and Swoboda, M., 2009. "Active Control of Corner Vortices on a Highly Loaded Compressor Cascade". *8<sup>th</sup> European Turbomachinery Conference, Graz*.
- [10] Hecklau, M., Zander, V., Peltzer, I., Nitsche, W., Huppertz, A., and Swoboda, M., 2010. "Experimental AFC Approaches on a Highly Loaded Compressor Cascade". In *Active Flow Control II - NNFM*, King, R., ed., Springer.
- [11] Gmelin, C., Steger, M., Wassen, E., and Thiele, F., 2010. "Unsteady rans simulations of active flow control on turbomachinery blades". In *Active Flow Control II - NNFM*, King, R., ed., Springer.
- [12] Gmelin, C., Steger, M., Thiele, F., Huppertz, A., and Swoboda, M., 2010. "Unsteady RANS Simulations of a Highly Loaded Low Aspect Ratio Compressor Cascade with Active Flow Control". *ASME GT2010-22516*.
- [13] Gmelin, C., Steger, M., Wassen, E., Thiele, F., Huppertz, A., and Swoboda, M., 2010. "Unsteady RANS Simulations on Flow Control in a Compressor Cascade using Pulsed Jets at the Blade". *AIAA Paper 2010-4588*.
- [14] Gmelin, C., Steger, M., Zander, V., Nitsche, W., Thiele,

- F., Huppertz, A., and Swoboda, M., 2010. "Numerical Investigations of Active Flow Control using Synthetic Jets on a Highly Loaded Compressor Stator Cascade". *ASME FEDSM-ICNMM2010-30725*.
- [15] Hecklau, M., Wiederhold, O., Zander, V., King, R., Nitsche, W., Huppertz, A., and Swoboda, M., 2010. "Active Separation Control with Pulsed Jets in a Critically Loaded Compressor Cascade". *AIAA Paper 2010-4252*.
- [16] Hecklau, M., Gmelin, C., Nitsche, W., Thiele, F., Huppertz, A., and Swoboda, M., 2011. "Experimental and Numerical Results of AFC on a Highly Loaded Stator Cascade". *9<sup>th</sup> European Turbomachinery Conference, Istanbul, Turkey (submitted)*.
- [17] Zander, V., Hecklau, M., Nitsche, W., Huppertz, A., and Swoboda, M., 2011. "Active flow control by means of synthetic jets on a highly loaded compressor cascade". *9<sup>th</sup> European Turbomachinery Conference, Istanbul (submitted)*.
- [18] Zander, V., Dobriloff, C., Lumpe, M., and Nitsche, W., 2011. "Wall shear stress measurements on a highly loaded compressor cascade". *ASME GT2011-46364 (submitted)*.
- [19] Hartsel, J. E., 1972. "Prediction of effects of mass-transfer cooling on the blade row efficiency of turbine airfoils". *AIAA 10th Aerospace Sciences Meeting, San Diego, California*.
- [20] Bräunling, W.J.G., 2009. *Flugzeugtriebwerke*. Springer.
- [21] NUMECA International, 2007. *FINE<sup>TM</sup>/Turbo v8, User Manual*. NUMECA Int., Brussels.
- [22] Spalart, P.R., and Allmaras, S.R., 1992. "A One-Equation Turbulence Model for Aerodynamic Flows". *AIAA 92-0439*.
- [23] Weber, A., 2008. *G3DMESH v4.5.4*. DLR, Institut für Antriebstechnik, Köln.
- [24] Hunt, J.C.R., Wray, A.A., and Moin, P., 1988. "Eddies, Stream, and Convergence Zones in Turbulent Flows". *Technical Report CTR-S88, Center for Turbulence Research*.
- [25] Lewin, E., Kozulovic, D., and Stark, U., 2010. "Experimental and Numerical Analysis of Hub-Corner Stall in Compressor Cascades". *ASME GT2010-22704*.
- [26] Liesner, K., Meyer, R., Lemke, M., Gmelin, C., and Thiele, F., 2010. "On the Efficiency of Secondary Flow Suction in a Compressor Cascade". *ASME GT2010-22336*.